One-step Mechanochemical Incorporation of an Insoluble Cesium Additive for High Performance Planar Heterojunction Solar Cells

Daniel Prochowicz,[*,a,b] *Pankaj Yadav,*[a,c] *Michael Saliba,*[a,d] *Dominik J. Kubicki,*[a,e] *Mohammad Mahdi Tavakoli,*[a,f] *Shaik M. Zakeeruddin,*[a] *Janusz Lewiński,*[b,g] *Lyndon Emsley*[e] *and Michael Grätzel*[*,a]

[a] Laboratory of Photonics and Interfaces, Institute of Chemical Sciences and Engineering, School of Basic Sciences, Ecole Polytechnique Fédérale de Lausanne (EPFL), CH-1015 Lausanne, Switzerland

[b] Institute of Physical Chemistry, Polish Academy of Sciences, Kasprzaka 44/52, 01-224 Warsaw, Poland

[c] Department of Solar Energy, School of Technology, Pandit Deendayal Petroleum University, Gandhinagar-382 007, Gujarat, India

[d] Adolphe Merkle Institute, University of Fribourg, Chemin des Verdiers 4, CH-1700 Fribourg, Switzerland

[e] Laboratory of Magnetic Resonance, Institute of Chemical Sciences and Engineering, Ecole Polytechnique Fédérale de Lausanne (EPFL), CH-1015 Lausanne, Switzerland

[f] Department of Electrical Engineering and Computer Science, Massachusetts Institute of Technology, Cambridge, MA 02139, USA

[g] Faculty of Chemistry, Warsaw University of Technology, Noakowskiego 3, 00-664 Warsaw, Poland

AUTHOR INFORMATION

Corresponding Author

E-mail: dprochowicz@ichf.edu.pl, michael.graetzel@epfl.ch

ABSTRACT State-of-the-art cesium-containing multiple-cation perovskites are generally synthesized from stock solutions of perovskite precursors and CsI in DMSO and DMF. However, compositional diversity of multi-component perovskites is significantly hampered due to the poor solubility of other cesium halides in these solvents. Here, we show how insoluble CsCl, as a new source of cesium cation, can be integrated into a multiple-cation perovskite material by a one-step method involving grinding of the precursors. The resulting polycrystalline powder is fully soluble in a DMSO/DMF mixture and allows formation of perovskite thin films. ^{133}Cs solid-state MAS NMR data indicate that the cesium cation is almost fully (90%) incorporated into the 3D perovskite lattice, while the remaining 10% forms a cesium-rich mixed-halide secondary phase. The planar heterojunction device fabricated using this original mechanoperovskite yielded a power conversion efficiency of 19.12% and an open circuit voltage of 1.16 V. Moreover, we show that the introduction of chloride improves both interfacial and bulk photovoltaic metrics. Our one-step approach provides an efficient general method for incorporating poorly soluble salts into multi-component perovskite crystal lattices.

TOC GRAPHICS

Insert 2in×3in (5cm×7.5cm) graphic

The graphic for the TOC/Abstract should representative of your entire work and not be a duplicate of a graphic already used in the manuscript. Color structures, graphical images,

photographs, or reaction schemes are typically good choices.

Hybrid organic-inorganic metal halide perovskites have been attracting attention as promising materials for the next generation of solar cells, owing to their excellent optoelectronic properties including high light extinction coefficients,[1] long charge carrier diffusion lengths,[2,3,4] long charge carrier lifetimes and high charge carrier mobility.[5] In just a few years, perovskite solar cells (PSCs) have reached certified power conversion efficiencies (PCE) of over 22%, rivalling other well-established solar cell materials.[6,7] Within the diverse ABX_3 (A=Cs, MA, FA; B= Pb, Sn, Ge; X= Cl, Br, I) hybrid halide perovskites family, the most widely used materials are methylammonium lead iodide ($MAPbI_3$) and formamidinium lead iodide ($FAPbI_3$) and they are studied in both mesoporous and planar device architectures.[8] However, $MAPbI_3$ shows poor thermal and moisture stability[9] while $FAPbI_3$ suffers from thermodynamic instability, whereby it spontaneously transforms into a wide-bandgap hexagonal, yellow δ phase.[10,11] These shortcomings have been tackled by compositional engineering, for example, by mixing several monovalent A-site cations.[12,13,14,15] Double A-cation halide perovskites, in particular the $(FAPbI_3)_{0.85}(MAPbBr_3)_{0.15}$ (MAFA) composition, form stable 3D black perovskite phases and generally exhibit improved photovoltaic properties.[16,17,18,19] Remarkably, doping MAFA with inorganic cesium (Cs) cations helped to eliminate the δ-phase impurity and facilitated room temperature crystallization of the perovskite phase.[20] The resulting perovskites, with the general

formula $Cs_x(MA_{0.17}FA_{0.83})_{(100-x)}Pb(I_{0.83}Br_{0.17})_3$, were more thermally stable and less sensitive to processing conditions, enabling higher reproducibility.[20] These triple-cation compositions have been widely adopted in PSCs and are currently the subject of intense investigation.[21,22]

Cs-containing triple-cation perovskites are typically prepared by mixing a solution of CsI with a stock solution of MAFA perovskite precursors (see Scheme 1, *path 1*). The motivation for using CsI is that other cesium halides have poor solubility in DMSO and DMF, even at elevated temperatures. This solubility issue limits further progress in compositional engineering. More broadly, to increase diversity, it would be necessary to develop methods for integrating insoluble additives into multiple-cation perovskites. Mechanochemical synthesis has recently emerged as a straightforward, solvent-free method for preparing highly pure perovskites, providing rapid access to a variety of simple hybrid iodide and bromide perovskites[23,24,25,26] as well as phase pure mixed-cation perovskites.[27]

Here, we show that CsCl, which is insoluble in DMSO and DMF, can be integrated as a new source of Cs into a triple-cation perovskite composition using mechanochemistry. The resulting mechanoperovskite is fully soluble in a DMF/DMSO mixture and allows formation of thin films by a facile single-step deposition method (see Scheme 1, *path 2*). We show that such CsCl addition yields open circuit voltages (V_{oc}) as high as 1.16 V and leads to a power conversion efficiency (PCE) of 19.2% for a planar device. Moreover, we also analysed the effect of CsCl addition on the photovoltaic properties using electrochemical impedance spectroscopy (EIS) and the results indicate that such additive improves the interfacial and bulk electronic properties in planar PSCs.

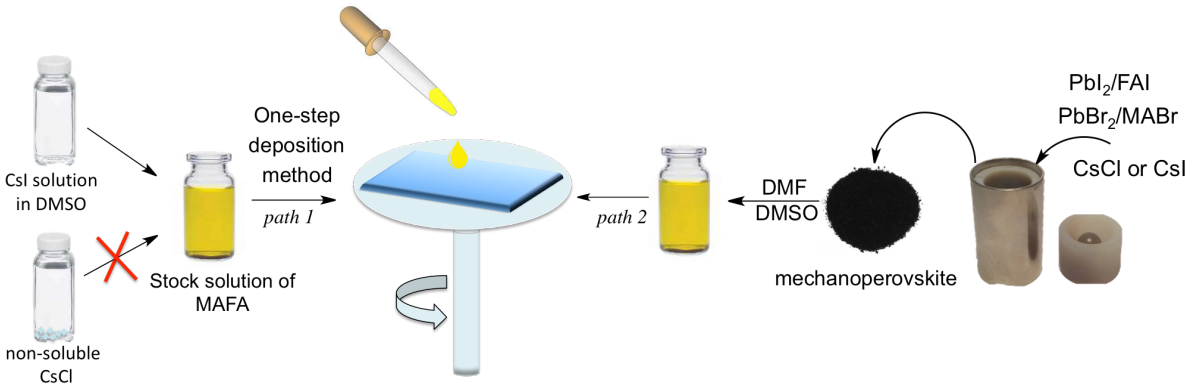

Scheme 1. Schematic representation of the one-step spin-coating deposition method using CsI and MAFA precursor solution (*path 1*), and powdered polycrystalline perovskites (*path 2*).

We first prepared the state-of-the-art triple-cation perovskite material (further referred to as **triple**) as a reference material by grinding the solid precursors according to a recently published procedure.[28] Here by replacing CsI with CsCl in a similar mechanosynthesis procedure, we obtained a new triple-cation mixed-halide perovskite (further referred to as **triple_Cl**) (see the ESI for details). The powder X-ray diffractograms (pXRD) of **triple** and **triple_Cl** (Figure S1) indicate that the two materials have a very similar structure, with the peaks at ~14.0° and ~28.0° originating from the (110) and (220) planes of a 3D perovskite phase. Both samples also exhibit a small peak at 12.6° corresponding to an excess of PbI_2, which was added to match the original composition of Saliba et al.[20] Next, both powders were dissolved in a mixture of DMF and DMSO (4:1 v/v), and the resulting solutions used to fabricate perovskite thin films by a single-step deposition method (further experimental details are given in the ESI). The pXRD patterns of the thus obtained films exhibit the expected black perovskite phase and PbI_2 reflections (Figure S2).

In order to evaluate the film quality, we characterized their morphology and optical properties. Plan view SEM images of both compositions reveal pinhole-free, uniform films after annealing at 100°C for 45 min (Figure S4). Previous reports have shown that the presence of chloride in the

starting solution leads to larger perovskite grains, thus enhancing the photovoltaic performance of the resulting devices.[29,30,31,32] Here, we find that **triple** and **triple_Cl** films exhibit a similar polycrystalline texture and comparable grain sizes in the range of 100–350 nm. This parameter being comparable in both compositions, we expect that any differences in performance will be largely caused by the charge carrier recombination and transfer dynamics across the heterojunction interfaces, rather than by morphological differences.[33] So far, studies of chlorine incorporation have been limited to single-cation lead halide perovskites ($MAPbI_3$ and $FAPbI_3$).[29,30,31] Since current best photovoltaic perovskite materials are multiple-cation compositions, here we seek to bridge this gap by investigating the effect of chloride addition in a triple-cation system.

Given the low chlorine content in the **triple_Cl** composition (~ 5 mol%), it is impossible to quantify by X-ray spectroscopy since the Cl Kα line (2.62 keV) overlaps with the much more intense Pb Mγ line (2.65 keV) with the resolution of EDX and XRF being on the order of 0.15 keV (the XRF spectrum of **triple_Cl** is given in Figure S5). Cesium incorporation into the perovskite lattice, on the other hand, can be confirmed in a straightforward manner with solid-state NMR, as we have previously demonstrated on **triple** and other similar compositions.[28,34] We have also demonstrated that the microstructure of bulk mechanochemical perovskites corresponds to that of thin films, which makes them a good candidate for high-sensitivity solid-state NMR studies.[28,35] We apply these notions here to probe the atomic-level microstructure of the cesium sites in the **triple_Cl** material. Figure 1 shows solid-state ^{133}Cs MAS NMR of the bulk mechanoperovskites. The quantitative spectrum of **triple_Cl** (Figure 1a) exhibits one main ^{133}Cs resonance which corresponds to cesium sites incorporated into the 3D perovskite lattice, coinciding with that of the previously reported **triple** composition (Figure 1b).[28] The spectrum

also shows a second, significantly smaller resonance whose quantification indicates that about 10% of cesium in the **triple_Cl** composition is present as a different phase. This resonance has a shift (103 ppm) corresponding to that of pure $CsPbBr_3$ (103 ppm) but it is significantly broader ((219 ± 9) Hz and about 2 kHz, respectively). Since the **triple_Cl** sample composition contains three anions (I, Br and Cl), the second phase is likely a mixed-anion cesium lead halide, similar to those formed by rubidium.[28] This is supported by analysing $CsPbBr_{1.5}Cl_{1.5}$ (Figure 1e) in which the disorder introduced by the presence of two X-site anions leads to a significantly broader ^{133}Cs resonance (fwhm of (2170 ± 30) Hz), as compared to pure $CsPbBr_3$ (fwhm: (219 ± 9) Hz) and $CsPbCl_3$ (fwhm: (192 ± 6) Hz). We exclude the presence of pure δ-$CsPbI_3$, which gives a peak at 240 ppm (Figure S5). The secondary phase in **triple_Cl** is most likely a mixed cesium lead chloride-bromide although the presence of small amounts of iodide cannot be excluded. Moreover, we cannot at this stage confirm the presence of chlorine in the main perovskite phase of **triple_Cl** by NMR (large quadrupolar couplings combined with low doping levels make ^{35}Cl solid-state NMR particularly challenging in perovskite materials; DNP has been used to observe low levels of chlorine in pharmaceutical formulations,[36] but due to the presence of extensive dynamics this is difficult to transfer to perovskites), making it difficult at present to accurately quantify the chemical composition of the main phase. Recently, the existence of Cl in a small proportion inside the methylammonium tri-halide tin perovskites was demonstrated.[37]

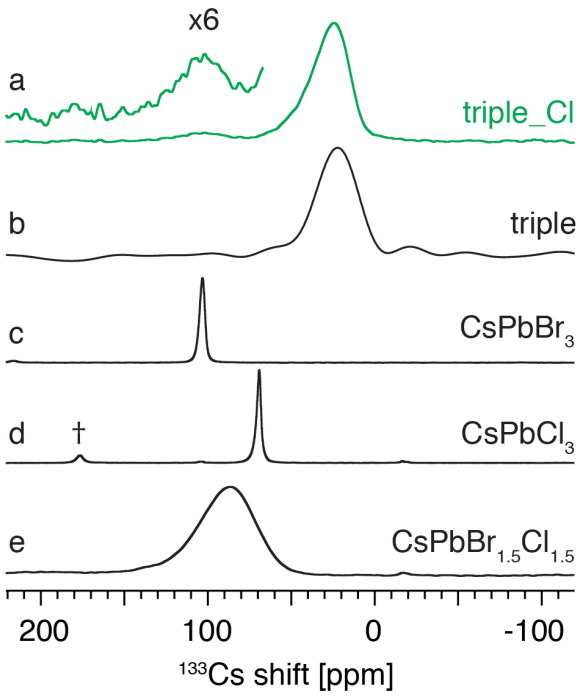

Figure 1. ^{133}Cs solid-state MAS NMR spectra of bulk (a) **triple_Cl**, (b) **triple**, (c) $CsPbBr_3$, (d) $CsPbCl_3$, (e) $CsPbBr_{1.5}Cl_{1.5}$ at 20 kHz MAS and 298 K. † is an impurity. The full spectra are given in Figure S6.

The possible incorporation of chlorine into the perovskite lattice together with the presence of a separate mixed-anion cesium lead halide phase should result in differences in the optical response and energy levels of **triple** and **triple_Cl**. The UV-VIS absorption spectra of the two thin films are presented in Figure 2a. The absorption onset of **triple** is at about 775.0 nm, consistent with the previously reported value.[20] The **triple_Cl** film exhibits a similar absorption spectrum with a small blue shift of 7-10 nm, indicating a wider bandgap (Figure 2a, inset). Extrapolated from the absorption of the direct transition at the absorption edge, the bandgap (E_g) of **triple** and **triple_Cl** was calculated as 1.58 eV and 1.60 eV, respectively. In addition, steady-state photoluminescence (PL) spectra show a blue shift of ~10 nm in **triple_Cl** compared to **triple** (Figure 2b), consistent with the UV-VIS measurements. We also note that the PL intensity

increased significantly in **triple_Cl** compared to **triple**, which indicates a decrease in non-radiative recombination originating from defects and trap states.

Ultraviolet photoelectron spectroscopy (UPS) was employed to investigate in more detail the energy levels of **triple** and **triple_Cl**. Figure 2c shows the UPS spectra of the two films, indicating their Fermi levels lie at 4.78 and 5.2 eV, respectively. The observed shift of the Fermi level by +0.42 eV indicates that **triple_Cl** is more p-type compared to the reference material. In addition, the calculated valence band positions: 5.58 eV (**triple**) and 5.72 eV (**triple_Cl**) indicate that the valence band is shifted by +0.14 eV in the Cl-contained material. Taken together, these results lead to a band diagram of **triple** and **triple_Cl** shown in Figure 2d. Since **triple_Cl** is well-matched with the TiO_2 electron-transporting layer, and is p-type nature, the electrical field at the interface can be stronger compared to **triple**, which may improve charge extraction in the final device.

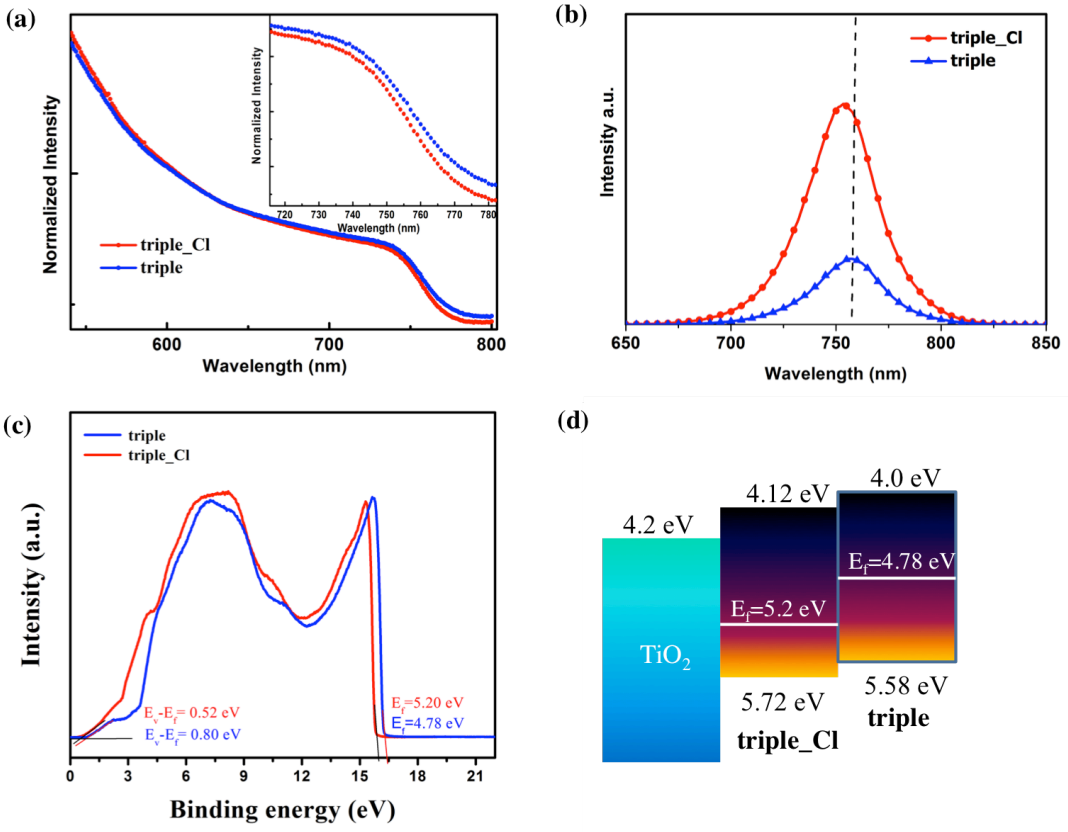

Figure 2. (a) UV–VIS absorption spectra and (b) steady-state photoluminescence spectra of **triple** and **triple_Cl** films. (c) UPS measurements of **triple** and **triple_Cl** films indicating the Fermi levels and the differences between valence band and Fermi level. (d) Schematic band diagram for the corresponding perovskite films.

To investigate the role of CsCl addition on the photovoltaic performance, we fabricated a batch of 20 planar structure devices in the following configuration: FTO/compact TiO_2/perovskite/Spiro-OMeTAD/Au. The cross-sectional SEM images of the as-fabricated PSCs show well-defined structures with an about 350 nm thick perovskite capping layer (Figure S7). The devices based on **triple** and **triple_Cl** yield average PCEs of 18.03±0.8 % and 18.62±0.5 %, respectively. The best **triple** device exhibits PCE of 18.83%, V_{OC} of 1.12 V, J_{SC} of 22.68 mA/cm^2 and FF of 73.4%, while the best **triple_Cl** device displays a PCE of 19.12%, V_{OC} of 1.16 V, J_{SC} of 22.54 mA/cm^2 and FF of 71.1%. The corresponding *J–V* characteristics are shown in Figure 3a (for the reproducibility and statistics histogram of all collected photovoltaic parameters see Figure S9).

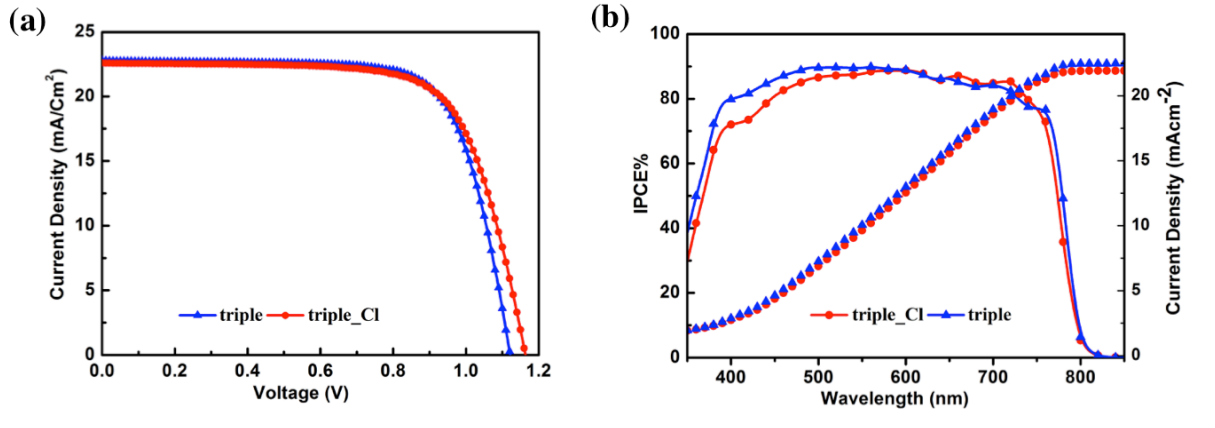

Figure 3. (a) *J-V* characteristics of the champion **triple** and **triple_Cl** PSCs recorded under standard 1 sun illumination, and (b) the corresponding IPCE spectra.

The higher PCE of the **triple_Cl** device is mainly due to its higher V_{oc} (1.16 V), compared to that of the **triple** device (1.12 V), which is among the highest V_{oc} reported for TiO_2-based planar-

architecture PSCs. The improvement in V_{OC} of **triple_Cl** devices (~40 mV) is larger than expected simply from the increased bandgap. Another contributing factor may be the reduced electron-hole recombination, which we discuss below. Notably, both PSCs show similar extent of *J–V* hysteresis behaviour (Figure S8), which is typical in TiO_2-based planar device architectures.[38,39] The incident photon-to-current efficiency (IPCE) spectra of both devices were measured and shown in Figure 3b. The integrated J_{sc} from the IPCE measurements match well those extracted from the *J–V* curves. Moreover, the blue-shifted trend of the absorption edge in IPCE coincides with that observed in the UV-VIS spectra (Figure 2a).

To gain further insight into the improvement in V_{oc}, we applied electrochemical impedance spectroscopy (EIS) to the fabricated devices. Figure S10 shows the Nyquist spectra of the **triple** and **triple_Cl** devices measured under illumination as a function of applied bias. Figure 4a illustrates the extracted value of R_{rec} from the low frequency spectra in a bias range from maximum power voltage to V_{oc}. Recently, we have demonstrated that the values of R_{rec} are inversely proportional to the recombination rate in PSCs.[40,41] The values of R_{rec} were obtained from the electrically equivalent circuit (Figure S11), comprising contributions from the series resistance (R_s), transport recombination (R_1), bulk capacitance (C_1) and the interfacial charge accumulation capacitance (C_{acc}). Figure 4a shows that the higher value of R_{rec} for the **triple_Cl** devices at bias close to V_{oc} and is consistent with lower recombination, leading to higher V_{oc}.

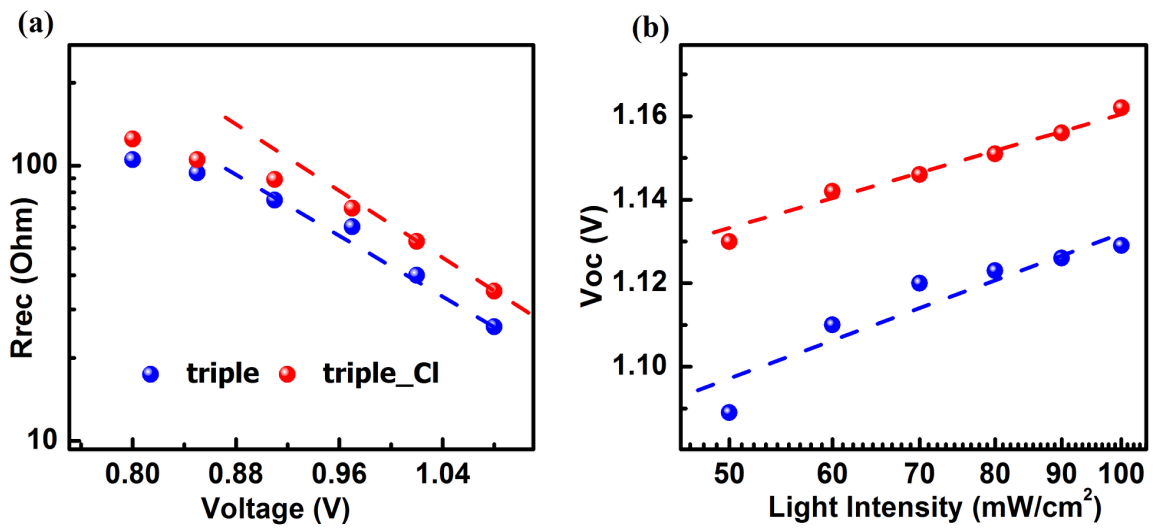

Figure 4. (a) Recombination resistance (R_{rec}) as a function of applied bias (V) under illumination; (b) open-circuit voltage (V_{oc}) as a function of light-intensity for **triple** and **triple_Cl** devices.

We note that suppressed recombination resulting from chlorine doping has also been observed by other authors.[29,32] There, the improvement is ascribed to an increase in the perovskite grain size, which is different from the present study, as we did not find any significant changes in the morphology and grain size distribution of the two materials. This result indicates that the presence of a minor mixed-anion cesium lead halide phase changes the intrinsic electrical properties of the perovskite material in an advantageous manner.

These results are further confirmed by measuring the V_{oc} as a function of illumination for **triple** and **triple_Cl** devices as shown in Figure 4b. The plot of V_{oc} vs log scaled illumination was fitted by a liner expression of $V_{oc} = n\left({}^{K_B T}/_{q}\right)\ln(I) + Constant$, where n is the ideality factor, K_B is the Boltzmann constant, T is the absolute temperature, q is the charge and I is the illumination intensity. The n value of 1.62 for **triple_Cl** and a higher n value of 1.7 for **triple** device were calculated. This results in reduced nonradioactive recombination and higher V_{OC} for **triple_Cl** device. A recent study by Jin et al. has demonstrated that a strong electrostatic

attraction between Cl and MA^+ is beneficial for chemical stability and recombination kinetics.[42,43] Furthermore, we measured the *J-V* characteristics in the dark and in forward direction for **triple** and **triple_Cl** devices (Figure S12). The lower leakage current in the exponential region and lower slope in the high forward bias region for **triple_Cl** further confirms the lower recombination losses and R_S.

In conclusion, we have addressed the problem of integrating poorly soluble alkali metal salts into multiple-cation perovskite materials using one of the best performing composition to date. We have shown that Cs was incorporated into the A-site of the perovskite structure using an insoluble CsCl (90% Cs incorporation) by straightforward one-step grinding of the precursors, however the fate of Cl is at this stage unknown. Moreover, we demonstrate that the improved V_{oc} and PCE in the **triple_Cl** material is caused by supressed recombination at interfaces, rather than by morphological differences. This new method of incorporation of dopants insoluble in DMSO and DMF is expected to be quite general, and will relieve the previous limitation on diversity in multi-component perovskites.

ASSOCIATED CONTENT

Supporting Information

The Supporting Information is available free of charge on the ACS Publications website.

Sample preparation and characterization; pXRD patterns of mechanoperovskites and thin films; SEM plan view and cross-sectional images; Full ^{133}Cs MAS NMR spectra; *J-V* hysteresis characteristics of the devices; statistics histogram; Nyquist spectra of the devices under light at zero bias; current-voltage plot of PSCs measured under dark in forward direction scan. (PDF)

Notes

The authors declare no competing financial interest

ACKNOWLEDGMENT

D. P. acknowledges support from the Marie Skłodowska Curie fellowship, H2020 Grant agreement no. 707168. M. S. acknowledges support from the co-funded Marie Skłodowska Curie fellowship, H2020 Grant agreement no. 665667. J. L. and M. G. thank funding from the European Union's Horizon 2020 programme, through a FET Open research and innovation action under grant agreement no. 687008. This work was supported by ERC Advanced Grant No. 320860 and Swiss National Science Foundation Grant No. 200021_160112.

References

(1) Lin, Q.; Armin, A.; Nagiri, R. C. R.; Burn, P. L.; Meredith, P. Electrooptics of perovskite solar cells. *Nat. Photonics* **2015**, *9*, 106-112.

(2) Stranks, S. D.; Eperon, G. E.; Grancini, G.; Menelaou, C.; Alcocer, M. J.; Leijtens, T.; Herz, L. M.; Petrozza, A.; Snaith, H. J. Electron-hole Diffusion Lengths Exceeding 1 Micrometer in an Organometal Trihalide Perovskite Absorber. *Science* **2013**, *342*, 341-344.

(3) Dong, Q. F.; Fang, Y. J.; Shao, Y. C.; Mulligan, P.; Qiu, J.; Cao, L.; Huang, J. S. Electron-hole Diffusion Lengths > 175 μm in Solution-Grown $CH_3NH_3PbI_3$ Single Crystals. *Science* **2015**, *347*, 967−970.

(4) Shi, D.; Adinolfi, V.; Comin, R.; Yuan, M. J.; Alarousu, E.; Buin, A.; Chen, Y.; Hoogland, S.; Rothenberger, A.; Katsiev, K.; Losovyj, Y.; Zhang, X.; Dowben, P. A.; Mohammed, O. F.; Sargent, E. H.; Bakr, O. M. Low trap-state density and long carrier diffusion in organolead trihalide perovskite single crystals. *Science* **2015**, *347*, 519-522.

(5) Wehrenfennig, C.; Eperon, G. E.; Johnston, M. B.; Snaith, H. J.; Herz, L. M. High Charge Carrier Mobilities and Lifetimes in Organolead Trihalide Perovskites. *Adv. Mater.* **2014**, *26*, 1584-1589.

(6) Yang, W. S.; Park, B.-W.; Jung, E. H.; Jeon, N. J.; Kim, Y. C.; Lee, D. U.; Shin, S. S.; Seo, J.; Kim, E. K.; Noh, J. H.; et al. Iodide Management in Formamidinium-Lead-Halide-Based Perovskite Layers for Efficient Solar Cells. *Science* **2017**, *356*, 1376−1379.

(7) https://www.nrel.gov/pv/assets/images/efficiency-chart.png

(8) Zhao, Y.; Zhu, K. Organic–Inorganic Hybrid Lead Halide Perovskites for Optoelectronic and Electronic Applications. *Chem. Soc. Rev.* **2016**, *45*, 655-689.

(9) Conings, B.; Drijkoningen, J.; Gauquelin, N.; Babayigit, A.; D'Haen, J.; D'Olieslaeger, L.; Ethirajan, A.; Verbeeck, J.; Manca, J.; Mosconi, E.; de Angelis, F.; Boyen, H.-G. Intrinsic Thermal Instability of Methylammonium Lead Trihalide Perovskite. *Adv. Energy Mater.* **2015**, *5*, 1500477.

(10) Eperon, G. E.; Stranks, S. D.; Menelaou, C.; Johnston, M. B.; Herz, L. M.; Snaith, H. J. Formamidinium lead trihalide: a broadly tunable perovskite for efficient planar heterojunction solar cells. *Energy Environ. Sci*. **2014**, *7*, 982–988.

(11) Lee, J. W.; Seol, D. J.; Cho, A. N.; Park, N. G. High-Efficiency Perovskite Solar Cells Based on the Black Polymorph of $HC(NH_2)_2PbI_3$. *Adv. Mater*. **2014**, *26*, 4991–4998.

(12) Pellet, N.; Gao, P.; Gregori, G.; Yang, T. Y.; Nazeeruddin, M. K.; Maier, J.; Grätzel, M. Mixed-Organic-Cation Perovskite Photovoltaics for Enhanced Solar-Light Harvesting. *Angew. Chem. Int. Ed*. **2014**, *53*, 3151–3157.

(13) Yang, Z.; Chueh, C. C.; Liang, P. W.; Crump, M.; Lin, F.; Zhu, Z.; Jen, A. K. Y. Effects of formamidinium and bromide ion substitution in methylammonium lead triiodide toward high-performance perovskite solar cells. *Nano Energy* **2016**, *22*, 328–337.

(14) Yi, C.; Luo, J.; Meloni, S.; Boziki, A.; Ashari-Astani, N.; Grätzel, C.; Zakeeruddin, S. M.; Röthlisberger, U.; Grätzel, M. Entropic stabilization of mixed A-cation ABX_3 metal halide perovskites for high performance perovskite solar cells. *Energy Environ. Science*, **2016**, *9*, 656-662.

(15) Lee, J.-W.; Kim, D.-H.; Kim, H.-S.; Seo, S.-W.; Cho, S. M.; Park, N.-G. Formamidinium and Cesium Hybridization for Photo- and Moisture-Stable Perovskite Solar Cell. *Adv. Energy Mater*. **2015**, *5*, 1501310.

(16) Jeon, N. J.; Noh, J. H.; Yang, W. S.; Kim, Y. C.; Ryu, S.; Seo, J.; Seok, S. I. Compositional engineering of perovskite materials for high-performance solar cells. *Nature* **2015**, *517*, 476–480.

(17) Bi, D.; Tress, W.; Dar, M. I.; Gao, P.; Luo, J.; Renevier, C.; Schenk, K.; Abate, A.; Giordana, F.; Baena, J. C.; Decoppet, J. D.; Zakeeruddin, S. M.; Nazeeruddin, M. K.; Grätzel, M.; Hagfeldt, A. Efficient Luminescent Solar Cells Based on Tailored Mixed-Cation Perovskites. *Sci. Adv*. **2016**, *2*, e1501170.

(18) Li, X.; Bi, D. Q.; Yi, C. Y.; Decoppet, J. D.; Luo, J. S.; Zakeeruddin, S. M.; Hagfeldt, A.; Grätzel, M. A Vacuum Flash-Assisted Solution Process for High-Efficiency Large-Area Perovskite Solar Cells. *Science* **2016**, *353*, 58−62.

(19) Jiang, Q.; Chu, Z.; Wang, P.; Yang, X.; Liu, H.; Wang, Y.; Yin, Z.; Wu, J.; Zhang, X.; You. J. Planar-Structure Perovskite Solar Cells with Efficiency beyond 21%. *Adv. Mater*. **2017**, 1703852.

(20) Saliba, M.; Matsui, T.; Seo, J. Y.; Domanski, K.; Correa-Baena, J. P.; Nazeeruddin, M. K.; Zakeeruddin, S. M.; Tress, W.; Abate, A.; Hagfeldt, A.; Grätzel, M. Cesium-containing triple cation perovskite solar cells: improved stability, reproducibility and high efficiency. *Energy Environ. Sci.* **2016**, *9*, 1989–1997.

(21) Anaraki, E. H.; Kermanpur, A.; Steier, L.; Domanski, K.; Matsui, T.; Tress, W.; Saliba, M.; Abate, A.; Grätzel, M.; Hagfeldt, A.; Correa- Baena, J. P. Highly Efficient and Stable Planar Perovskite Solar Cells by Solution-Processed Tin Oxide. *Energy Environ. Sci*. **2016**, *9*, 3128-3134.

(22) Song, J.; Liu, L.; Wang, X.-F.; Chen, G.; Tian, W.; Miyasaka, T. Highly efficient and stable low-temperature processed ZnO solar cells with triple cation perovskite absorber. *J. Mater. Chem. A* **2017**, *5*, 13439-13447.

(23) Prochowicz, D.; Franckevicius, M.; Cieślak, A. M.; Zakeeruddin, S. M.; Graetzel, M.; Lewiński, J. Mechanosynthesis of the Hybrid Perovskite $CH_3NH_3PbI_3$: Characterization and the Corresponding Solar Cell Efficiency. *J. Mater. Chem. A* **2015**, *3*, 20772-20777.

(24) Prochowicz, D.; Yadav, P.; Saliba, M.; Saski, M.; Zakeeruddin, S. M.; Lewinski, J.; Grätzel, M. Reduction in the Interfacial Trap Density of Mechanochemically-Synthesized $MAPbI_3$. *ACS Appl. Mater. Interfaces* **2017**, *34*, 28418–28425.

(25) Jodlowski, A. D.; Ypez, A.; Luque, R.; Camacho, L.; de Miguel, G. Benign-by-Design Solventless Mechanochemical Synthesis of Three-, Two-, and One-Dimensional Hybrid Perovskites. *Angew. Chem. Int. Ed*. **2016**, *55*, 14972-14977.

(26) Pal, P.; Saha, S.; Banik, A.; Sarkar, A.; Biswas, K. All-Solid-State Mechanochemical Synthesis and Post-Synthetic Transformation of Inorganic Perovskite-type Halides. *Chem. Eur. J*. **2018**, *24*, 1811-1815.

(27) Prochowicz, D.; Kumar, P.; Saliba, M.; Saski, M.; Zakeeruddin, S. M.; Lewiński, J.; Grätzel, M. Mechanosynthesis of pure phase mixed-cation $MA_xFA_{1-x}PbI_3$ hybrid perovskite: Characterization and the corresponding photovoltaic performance. *Sustainable Energy Fuels* **2017**, *1*, 689–693.

(28) Kubicki, D. J.; Prochowicz, D.; Hofstetter, A.; Zakeeruddin, S. M.; Grätzel, M.; Emsley, L. Phase Segregation in Cs-, Rb- and K-Doped Mixed-Cation $(MA)_x(FA)_{1-x}PbI_3$ Hybrid Perovskites from Solid-State NMR. *J. Am. Chem. Soc*. **2017**, *139*, 14173–14180.

(29) Fan, L; Ding, Y.; Luo, J.; Shi, B.; Yao, X.; Wei, C.; Zhang, D.; Wang, G.; Sheng, Y.; Chen, Y.; Hagfeldt, A.; Zhao, Y.; Zhang, X. Elucidating the Role of Chlorine in Perovskite Solar Cells. *J. Mater. Chem. A*, **2017**, *5*, 7423-7432.

(30) Xu, F.; Zhang, T.; Li, G.; Zhao, Y. Synergetic Effect of Chloride Doping and $CH_3NH_3PbCl_3$ on $CH_3NH_3PbI_{3-x}Cl_x$ Perovskite-Based Solar Cells. *ChemSusChem* **2017**, *10*, 2365-2369.

(31) Liang, P.-W.; Chueh, C.-C.; Xin, Q.-K.; Zuo, F.; Williams, S. T.; Liao, C.-Y.; Jen, A. K.-Y. High-Performance Planar-Heterojunction Solar Cells Based on Ternary Halide Large-Band-Gap Perovskites. *Adv. Energy Mater*. **2015**, *5*, 1400960.

(32) Xu, Y.; Zhu, L.; Shi, J.; Lv, S.; Xu, X.; Xiao, J.; Dong, J.; Wu, H.; Luo, Y.; Li, D.; Meng, Q. Efficient Hybrid Mesoscopic Solar Cells with Morphology-Controlled $CH_3NH_3PbI_{3-x}Cl_x$ Derived from Two-Step Spin Coating Method. *ACS Appl. Mater. Interfaces* **2015**, *7*, 2242–2248.

(33) Chen, Q.; Zhou, H.; Fang, Y.; Stieg, A. Z.; Song, T.-B.; Wang, H.-H.; Xu, X.; Liu, Y.; Lu, S.; You, J.; Sun, P.; McKay, J.; Goorsky, M. S.; Yang, Y. The optoelectronic role of chlorine in $CH_3NH_3PbI_3$(Cl)-based perovskite solar cells. *Nature Commun*. **2015**, *6*, 7269.

(34) Kubicki, D.; Prochowicz, D.; Hofstetter, A.; Pechy, P.; Zakeeruddin, S. M.; Graetzel, M.; Emsley, L. Cation Dynamics in Mixed-Cation $(MA)_x(FA)_{1-x}PbI_3$ Hybrid Perovskites from Solid-State NMR. *J. Am. Chem. Soc*. **2017**, *139*, 10055−10061.

(35) Kubicki, D.: Prochowicz, D.; Hofstetter, A.; Saski, M.; Yadav, P.; Bi, D.; Pellet, N.; Lewiński, J.; Zakeeruddin, S. M.; Grätzel, M.; Emsley, L. Formation of stable mixed guanidinium-methylammonium phases with exceptionally long carrier lifetimes for high efficiency lead iodide-based perovskite photovoltaics. *J. Am. Chem. Soc*. **2018**, DOI: 10.1021/jacs.7b12860.

(36) Hirsh, D. A.; Rossini, A. J.; Emsley, L.; Schurko, R. W. ^{35}Cl dynamic nuclear polarization solid-state NMR of active pharmaceutical ingredients. *Phys. Chem. Chem. Phys*. **2016**, *18*, 25893-25904.

(37) Cheng-Min Tsai, Nayantara Mohanta, Chi-Yung Wang, Yu-Pei Lin, Yaw-Wen Yang, Chien-Lung Wang, Chen-Hsiung Hung, and Eric Wei-Guang Diau, *Angew. Chem. Int. Ed*. **2017**, 56, 13819 –13823.

(38) Mu, C.; Pan, J.; Feng, S.; Li, Q.; Xu, D. Quantitative Doping of Chlorine in Formamidinium Lead Trihalide ($FAPbI_{3-x}Cl_x$) for Planar Heterojunction Perovskite Solar Cells. *Adv. Energy Mater*. **2017**, *7*, 1601297.

(39) Unger, E. L.; Hoke, E. T.; Bailie, C. D.; Nguyen, W. H.; Bowring, A. R.; Heumuller, T.; Christoforo, M. G.; McGehee, M. D. Hysteresis and Transient Behavior in Current–Voltage Measurements of Hybrid-Perovskite Absorber Solar Cells. *Energy Environ. Sci*. **2014**, *7*, 3690-3698.

(40) Yadav, P.; Dar, M.; Arora, N.; Alharbi, E. A.; Giordano, F.; Zakeeruddin, S. M.; Grätzel, M. The Role of Rubidium in Multiple-Cation-Based High-Efficiency Perovskite Solar Cells. *Adv. Mater*. **2017**, *29*, 1701077.

(41) Yadav, P.; Alotaibi, M. H.; Arora, N.; Dar, M. I.; Zakeeruddin, S. M.; Grätzel, M. Influence of the Nature of A Cation on Dynamics of Charge Transfer Processes in Perovskite Solar Cells. *Adv. Funct. Mater*. **2018**, 1706073.

(42) Xie, L.-Q.; Zhang, T.-Y.; Chen, L.; Guo, N.; Wang, Y.; Liu, G.-K.; Wang, J.-R.; Zhou, J.-Z.; Yan, J.-W.; Zhao, Y.-X.; Mao, B.-W.; Tian, Z.-Q. Organic–inorganic interactions of single crystalline organolead halide perovskites studied by Raman spectroscopy. *Phys. Chem. Chem. Phys*. **2016**, *18*, 18112-18118.

(43) Jin, J.; Li, H.; Chen, C.; Zhang, B.; Xu, L.; Dong, B.; Song, H.; Dai, Q. Enhanced Performance of Perovskite Solar Cells with Zinc Chloride Additives. *ACS Appl. Mater. Interfaces* **2017**, *9*, 42875−42882.